Gomez Paez, Shirley; Martinez, Camilo; Herrera, William J.; Levy Yeyati, Alfredo; Burset, Pablo

Dirac point formation revealed by Andreev tunneling in superlattice-graphene/superconductor junctions

Published in:
Physical Review B

DOI:
10.1103/PhysRevB.100.205429

Published: 27/11/2019

Document Version
Publisher's PDF, also known as Version of record

Please cite the original version:
Gomez Paez, S., Martinez, C., Herrera, W. J., Levy Yeyati, A., & Burset, P. (2019). Dirac point formation revealed by Andreev tunneling in superlattice-graphene/superconductor junctions. *Physical Review B*, *100*(20), 1-9. Article 205429. https://doi.org/10.1103/PhysRevB.100.205429

Dirac point formation revealed by Andreev tunneling in superlattice-graphene/superconductor junctions

Shirley Gómez Páez,[1,2] Camilo Martínez,[1] William J. Herrera,[1] Alfredo Levy Yeyati,[3] and Pablo Burset[4]

[1]*Departamento de Física, Universidad Nacional de Colombia, 111321 Bogotá, Colombia*

[2]*Departamento de Física, Universidad el Bosque, 110121 Bogotá, Colombia*

[3]*Departamento de Física Teórica de la Materia Condensada, Condensed Matter Physics Center (IFIMAC), and Instituto Nicolás Cabrera, Universidad Autónoma de Madrid, 28049 Madrid, Spain*

[4]*Department of Applied Physics, Aalto University, 00076 Aalto, Finland*

(Received 11 July 2019; published 27 November 2019)

A graphene superlattice is formed by a one-dimensional periodic potential and is characterized by the emergence of new Dirac points in the electronic structure. The group velocity of graphene's massless Dirac fermions at the new points is drastically reduced, resulting in a measurable effect in the conductance spectroscopy. We show here that tunnel spectroscopy using a superconducting hybrid junction is more sensitive to the formation of Dirac points in the spectrum of graphene superlattices due to the additional contribution of Andreev processes. We examine the transport properties of a graphene-based superlattice-superconductor hybrid junction and demonstrate that a superlattice potential can coexist with proximity-induced superconducting correlations. Both effects contribute to change graphene's spectrum for subgap energies, and as a result, the normalized tunneling conductance features sharp changes for voltages proportional to the energy separation between the original and newly generated Dirac points. Consequently, the superconducting differential conductance provides an excellent tool to reveal how the new Dirac points emerge from the original band. This result is robust against asymmetries and finite-size effects in the superlattice potential and is improved by an effective doping comparable to the superconducting gap.

DOI: 10.1103/PhysRevB.100.205429

I. INTRODUCTION

Graphene is a versatile material that can be modified to be metallic or semiconducting, owing to its gapless, linear low-energy spectrum [1–3]. This duality can be exploited in graphene superlattices, formed by a periodic, one-dimensional electrostatic potential on the graphene sheet, making graphene a promising candidate for designed electronic circuits. It is theoretically established that charge carriers in graphene behave like chiral Dirac fermions. Under a one-dimensional superlattice potential of amplitude U and period L (see Fig. 1), chirality forbids the opening of a band gap, instead creating new Dirac points (DPs) when the product UL reaches a critical value [4–6].

The propagation of chiral Dirac fermions under superlattices is highly anisotropic and can be controlled by varying the superlattice potential and Fermi energy. The resulting carrier velocity can be completely suppressed along one direction but is barely changed in the opposite, allowing for collimated electron beams [7]. Experimental realization of high-quality periodic superlattice potentials on graphene has been achieved using boron nitride encapsulation [8,9]. Dirac point formation was measured as resistivity peaks [10–12], paving the way for novel and exotic physics in graphene-based superlattices [13,14].

The recent discovery of unconventional superconductivity in bilayer graphene superlattices [14] has pointed to the interesting connection between superconducting correlations and superlattice potentials in graphene. However, to the best of our knowledge, the interplay between superconductivity and Dirac point formation by one-dimensional superlattices has not been explored yet. Graphene-superconductor hybrids can now be fabricated in high-quality transparent junctions that work in the ballistic regime [15–18]. In such hybrid junctions, electrons and holes from the conduction band of the normal lead combine to form Cooper pairs in the superconductor by means of a microscopic process known as Andreev reflection [19]. When the doping is smaller than the applied voltage and the superconducting gap, graphene's peculiar gapless dispersion allows for an unusual Andreev reflection where conduction band electrons are converted into holes belonging to the valence band [20]. Here, we demonstrate that these interband Andreev processes provide unique signatures of the formation of Dirac points, which could substantially facilitate their experimental detection.

Advances in experimental control of graphene devices are leading to a series of remarkable works reporting interband Andreev reflections [21], spectroscopy of Andreev bound states in Josephson junctions [22], splitting of Cooper pairs [23], and proximity-induced unconventional superconductivity [24–28]. Since a superlattice potential can be seen as a series of p-n junctions (see Fig. 1), an example of the potential applications of superlattice-superconductor hybrids is the recently measured [29] focusing of beams of Dirac fermions in graphene-based p-n junctions [30–32]. Existing theoretical works extend such effects to graphene junctions involving ferromagnets [33] and superconductors [34].

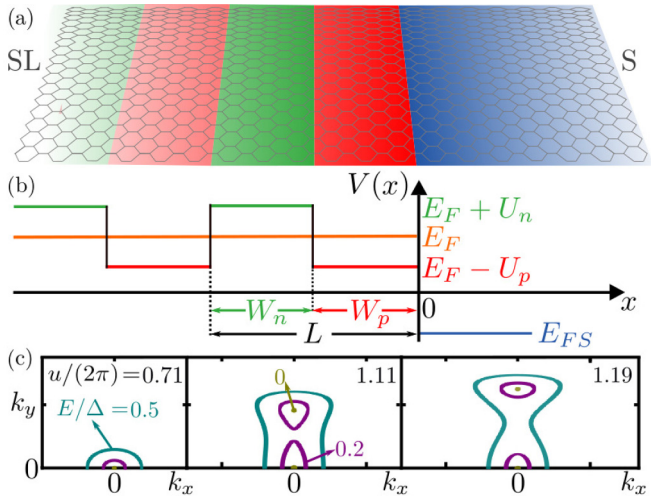

FIG. 1. (a) Semi-infinite superlattice (SL) coupled to a superconductor (S) on top of a graphene layer. (b) Sketch of the system's energy diagram. (c) Phase space contour plot showing the formation of a new Dirac point when the normalized barrier strength u reaches a resonance condition ($u = 2\pi$). See text for more details.

In this paper, we analyze the interplay between a superlattice potential and proximity-induced superconductivity on graphene. We focus on the effect of the emergence of new DPs on the transport properties of a graphene-based superlattice-superconductor (SL-S) junction. We demonstrate that subgap transport is extremely sensitive to the creation of new DPs when interband Andreev processes are dominant. Strikingly, the differential conductance presents sharp changes for voltages proportional to the energy separation between the original and the newly generated DPs. This effect is robust against asymmetries in the superlattice potential, the presence of an additional doping on the graphene layer, and finite-size effects. Therefore, graphene-based SL-S junctions are a convenient setup for addressing fundamental questions about the formation of new chiral Dirac fermions by periodic potentials and a promising component of future graphene-based electronic circuits with tailored properties.

II. DIFFERENTIAL CONDUCTANCE OF A GRAPHENE-BASED SUPERLATTICE-SUPERCONDUCTOR JUNCTION

We consider an infinite graphene plane where a superlattice potential $V(x)$ is created on the $x < 0$ region and superconductivity is induced by the proximity effect on the half plane with $x > 0$. The resulting graphene-based SL-S junction is sketched in Fig. 1. Assuming valley and spin degeneracy and zigzag edge termination, the Dirac–Bogoliubov–de Gennes (DBdG) Hamiltonian in sublattice and particle-hole (Nambu) spaces is given by [20,35,36]

$$\check{H}_{\rm DBdG} = \begin{pmatrix} \hat{h} + V(x)\hat{\sigma}_0 & \hat{\Delta}(x) \\ \hat{\Delta}^\dagger(x) & -\hat{h} - V(x)\hat{\sigma}_0 \end{pmatrix}, \tag{1}$$

with $\hat{h} = v_F(-i\partial_x\hat{\sigma}_1 + q\hat{\sigma}_2) - \epsilon\hat{\sigma}_0$ being the single-particle Dirac Hamiltonian, q being the conserved component of the wave vector parallel to the interface, v_F being the Fermi velocity, and $\hat{\sigma}_{0,1,2,3}$ being the Pauli matrices in sublattice space. The superlattice potential consists of a periodic repetition of potential barriers and wells with height $\pm U_{n,p}$ and width $W_{n,p}$ (see Fig. 1). Explicitly,

$$V(x) = \begin{cases} E_F + U_n, & x \in [mL, mL - W_n], \\ E_F - U_p, & x \in [mL - W_n, (m-1)L], \end{cases} \tag{2}$$

with $m = 0, -1, -2, \ldots$ and $L = W_n + W_p$ being the period of the superlattice potential.

We denote the Fermi energy in the superconducting regions as E_{FS}. We consider rigid boundary conditions for a conventional proximity-induced s-wave pairing $\hat{\Delta}(x) = \Delta\hat{\sigma}_0\Theta(x)$, with $\Delta > 0$ being the pairing amplitude and $\Theta(x)$ being the Heaviside step function. Approximating the spatial dependence of the pairing potential by a step function is valid as long as the Fermi wavelength of the quasiparticles in the superconductor is much smaller than the superconducting coherence length $\xi_0 = \hbar v_F/\Delta$, i.e., $E_{FS} \gg \Delta$.

The transport properties of the SL-S junction are encoded in the retarded Green's function $\check{g}^r_q(x, x') = \int dq e^{iq(y-y')}\check{g}^r_q(x, x', y, y')$, which satisfies the nonhomogeneous DBdG equation

$$[(E + i0^+)\check{I} - \check{H}_{\rm DBdG}]\check{g}^r_q(x, x') = \delta(x - x')\check{I}, \tag{3}$$

with $\check{I}$ being the identity matrix. A solution of Eq. (3) is obtained combining asymptotic solutions of Eq. (1) that obey the boundary conditions at the edges of a finite-length graphene sheet, following a generalization of the method developed in Refs. [35,37–45]. The Green's function for the SL can then be written as

$$\hat{g}_{\rm SL}(0^-, 0^-) = \frac{i}{2\hbar v_F C_n}\begin{pmatrix} 0 & 2C_n \\ 0 & M + \sqrt{J + M^2} \end{pmatrix}, \tag{4}$$

with

$$M = C_pC_n - D^2_{pn} - 1, \quad J = 4C_nC_p,$$

$$C_{p(n)} = \frac{c_{p(n)}\left(c^2_{n(p)} + d^2_{n(p)}\right) + c_{n(p)}}{c_pc_n + 1}, \; D_{pn} = \frac{id_pd_n}{c_pc_n + 1},$$

and

$$c_{n(p)} = \frac{e^{-i\alpha[\epsilon(\chi)]}(e^{2ik_x[\epsilon(\chi)]W_{n(p)}} - 1)}{1 + e^{-2i\alpha[\epsilon(\chi)]}e^{2ik_x[\epsilon(\chi)]W_{n(p)}}},$$

$$d_{n(p)} = \frac{e^{-ik_x[\epsilon(\chi)]W_{n(p)}}(1 + e^{-2i\alpha[\epsilon(\chi)]})}{1 + e^{-2i\alpha[\epsilon(\chi)]}e^{-2ik_x[\epsilon(\chi)]W_{p(n)}}}.$$

Here, $e^{\pm i\alpha_{e(h)}[\epsilon]} = \hbar v_F(k^{e(h)}_x[\epsilon] \pm iq)/(\epsilon \pm E)$, and $k^{e(h)}_x[\epsilon] = \sqrt{[(\epsilon + E)/\hbar v_F]^2 - q^2}$, with E and ϵ being the excitation and potential energies, respectively. We consider a transparent coupling between the superlattice and the superconductor. For more details of the calculations, we refer the reader to Appendix A.

The differential conductance depends on the potential difference between SL and S, $V = V_{\rm SL} - V_{\rm S}$, and can be written as

$$\sigma_{\rm S}(V) = \frac{\partial I}{\partial V} = \sigma_{\rm Q}(V) + \sigma_{\rm A}(V), \tag{5}$$

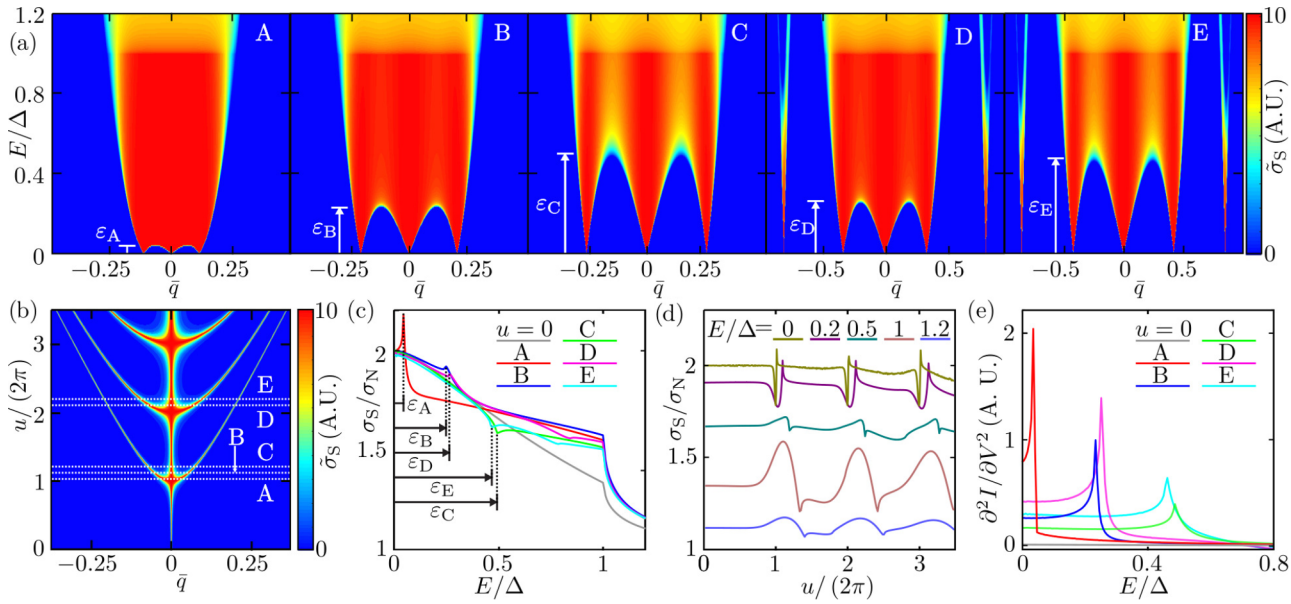

FIG. 2. Undoped, symmetric graphene superlattice. (a) Spectral differential conductance for different values of the superlattice potential (A) $u/(2\pi) = 1.03$, (B) 1.11, (C) 1.19, (D) 2.15, and (E) 2.23. (b) Map of the zero-energy spectral differential conductance as a function of u and $\bar{q} = q/q_{\max}$, with $\hbar v_F q_{\max} \simeq 29\Delta$. (c) Differential conductance as a function of the energy for the different values of u used in (a). The parameter ε indicates the separation of the new pair of Dirac points from the original cone. (d) Differential conductance as a function of u for different energies. (e) Estimation of ε from the second derivative of the current with respect to the voltage. For all cases $E_F = 0$ and $L = \xi_0/2$.

where σ_A (σ_Q) represents the contribution of the Andreev (quasiparticle) processes. Here,

$$\sigma_{Q(A)}(E) = 8\pi^2 \frac{e^2}{h} \int dq \tilde{\sigma}_{Q(A)}(E, q),$$

with $\tilde{\sigma}_{Q(A)}$ being defined in terms of the Green's functions in Appendix B. We normalize our results using the conductance for $\Delta = 0$, σ_N.

III. IDEAL SUPERLATTICE

We analyze the transport properties of a SL-S junction to illustrate how the emergence of Dirac points by the superlattice potential is neatly captured in the subgap differential conductance. We start considering an *ideal* superlattice potential, i.e., semi-infinite, created around the charge neutrality point, $E_F = 0$, and symmetric with $U_p = U_n \equiv U$ and $W_p = W_n = L/2$ (see Fig. 1). The normalized barrier strength is thus given by $u = UL/\hbar v_F$. Under these conditions, a new set of DPs is created when $u = 2n\pi$, with n being a positive integer [4–6].

As shown in Figs. 2(a) and 2(b), the superlattice potential can coexist with proximity-induced superconducting pairing in the superlattice region close to the interface with the superconductor. Indeed, the energy-momentum plots in Fig. 2(a), calculated for several values of the superlattice strength, clearly show how the band dispersion relation for subgap energies is modified after the first (panels A, B, C) and second (panels D, E) generations of DPs. The condition for the formation of DPs is thus not altered by the presence of the superconductor. Setting $E = 0$, we plot in Fig. 2(b) the spectral conductance $\sigma(E = 0, q)$ as a function of the transverse momentum $\hbar q$ and the barrier strength u. The first pair of DPs is formed at the critical value $u = 2\pi$, and the second is formed when $u = 4\pi$ is reached. The spectral density $\sigma(E, q)$ has been calculated in the SL region close to the interface with the superconductor. We identify the menorahlike structure of Fig. 2(b) as the fingerprint of the superlattice.

In the absence of the superlattice potential, a small trace of the original Dirac cone centered around $q = 0$ remains for energies below the superconducting gap Δ (cf. Refs. [46–48]). The superlattice potential changes the Fermi velocity, thus widening graphene's conelike spectrum, even before creating new DPs. Importantly, when coupled to a superconductor, the spectral density of states for subgap energies is higher compared to the nonsuperconducting case with $\Delta = 0$, which can be seen as a sharp change in color for energies below and above the gap in Fig. 2(a). Finally, as u increases beyond the critical value [panels A–C in Fig. 2(a)], a new pair of Dirac points appears. The original DP and the newly created ones are disconnected at zero energy, but they merge for finite energies over a characteristic value ε, indicated by white arrows in Fig. 2(a). The parameter ε becomes finite for $u > 2\pi$ and increases with u until it approaches Δ as a new pair of DPs is completely formed when $u = 4\pi$. At this critical value, ε is set to zero and becomes finite again when $u > 4\pi$. The energy parameter ε thus provides a qualitative measure of the separation between the original DP and every new pair.

These three effects, namely, (i) the formation of DPs when $u = 2n\pi$, (ii) an enhanced spectral density for subgap energies, and (iii) the separation between DPs characterized by the parameter ε, can be neatly observed in the normalized differential conductance σ_S/σ_N. Figures 2(c) and 2(d) show the normalized differential conductance of the SL-S junction as a function of the excitation energy and superlattice strength, respectively. In the absence of superlattice potential, since $E_F = 0$, we recover the conductance results of Ref. [20], where interband Andreev reflection is dominant (gray line

with $u = 0$). For $u \neq 0$, the normalized conductance at zero energy remains fixed at $2\sigma_0$, except at the critical values where DPs are formed [see Fig. 2(d)]. Since the normal-state conductance σ_0 accounts for the contribution from three channels, the doubling of the conductance is due to perfect Andreev reflection taking place at the original and new DPs.

By contrast, for finite energies we observe two effects connected to the presence of a superlattice potential. First, the conductance features a peak or a dip for energies equal to the parameter ε [see arrows in Fig. 2(c)]. Second, the superlattice increases the conductance for energies close to the gap ($E \lesssim \Delta$). The latter is a direct consequence of the superlattice-enhanced spectral density for subgap energies. The former can be associated with the different contributions from Andreev and normal reflections. For small values of ε, the normalized conductance exhibits a peak, indicating that interband Andreev processes become dominant when the DPs are created. As ε approaches Δ, the peak in the conductance becomes a dip since the DPs are more clearly separated, thus producing more backscattering for q values between DPs. In both cases, the parameter ε, which indicates the separation between the newly created DPs and the original band, is accessible through the differential conductance. By taking the derivative of the conductance with respect to the voltage (i.e., d^2I/dV^2), the small kinks in the conductance shown in Fig. 2(c) appear as clear peaks in the derivative [see Fig. 2(e)].

The above results show that a superlattice potential can create new DPs in the presence of superconducting correlations. As long as the strength of the potential is comparable to the superconducting gap, the zero-energy normalized conductance is completely dominated by interband Andreev processes and fixed to $2\sigma_0$. For finite energies, the normalized conductance features a sharp change at $E = \varepsilon$, which determines the energy separation between Dirac cones in the dispersion relation. The differential conductance of a SL-S junction and its derivative thus provide a very sensitive tool to study the creation of DPs by a superlattice potential.

IV. NONIDEAL SUPERLATTICE

We now consider three deviations from the ideal superlattice potential described above, namely, a finite doping on the graphene layer $E_F \neq 0$, an asymmetry in the superlattice potential, and a SL region of finite length.

A. Electrostatic asymmetry

We start analyzing the effect of asymmetry on the superlattice potential. First, we consider the effect of finite doping on the graphene layer with a perfectly symmetric SL potential with $U_n = U_p$ and $W_n = W_p$. Doping the graphene layer with $E_F \neq 0$ shifts the position where the new DPs are created [see Fig. 3(a)], but it does not change the condition for their formation, $u = 2n\pi$. If $E_F < \Delta$, shifting the position of the DP to finite energies results in an enhanced suppression of the conductance [see Figs. 3(b) and 3(c)] due to the vanishing density of states for holelike excitations [20,46]. This is a unique property of graphene's gapless spectrum which, interestingly, is not affected by the creation of new Dirac points, in contrast to the undoped case with $E_F = 0$ [compare Figs. 2(d) and 3(c)]. Since the splitting of the energy band into several DPs now takes place completely in the positive energy range (if $E_F > 0$), the range of energies where normal reflections are enhanced is now 2ε. As before, an analysis of the derivative of the conductance allows us to estimate the value of ε, corresponding to the change in slope in the conductance. Finite doping of the graphene layer, in the regime where interband Andreev reflections are enhanced, thus helps visualize the formation of DPs using the normalized conductance.

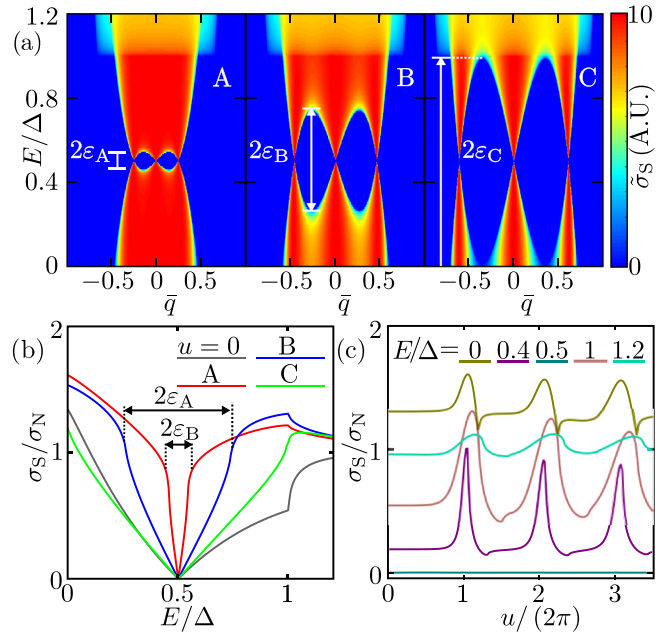

FIG. 3. Doped symmetric graphene superlattice. (a) Spectral differential conductance with $E_F = \Delta/2$ for different values of (A) $u/(2\pi) = 1.03$, (B) 1.11, and (C) 1.19. In all maps $\hbar v_F q_{\max} \simeq 16\Delta$. (b) Differential conductance as a function of the energy for the different values of u in (a). The arrows indicate the parameter ε. (c) Differential conductance as a function of u for different energies. In all cases $L = \xi_0/2$.

Asymmetry in the superlattice potential has an important effect on the formation of new DPs. The asymmetry may be induced by changing the relative height ($U_p \neq U_n$) or width ($W_p \neq W_n$) of the potential barriers and wells. We can thus parametrize it defining $\alpha = W_n/W_p$ and $\beta = U_n/U_p$. For an asymmetric superlattice, it is useful to define the average potential as the integral over a period [49], resulting in $E_F^* = E_F + \omega$, with $\omega = U_p(\alpha\beta - 1)/(1 + \alpha)$. The position of the original DP under an asymmetric superlattice is given by E_F^*, so we henceforth refer to it as the *effective* Fermi energy. It is now possible to redefine the potential in Eq. (2) as

$$V(x) = \begin{cases} E_F^* + \omega\frac{1+\beta}{\alpha\beta-1}, & x \in [mL, mL - W_n], \\ E_F^* - \omega\frac{\alpha+\alpha\beta}{\alpha\beta-1}, & x \in [mL - W_n, (m-1)L]. \end{cases} \tag{6}$$

For the case where the potential barriers and wells have the same width ($\alpha = 1$) but different heights ($\beta \neq 1$), following the sketch in Fig. 1, the barriers and wells take the values $E_F^* \pm \langle V \rangle$, respectively, with $\langle V \rangle = U_p(1 + \beta)/2$. The main effect of the asymmetry is to shift the Fermi energy to the effective one E_F^*, where the original Dirac cone is and the

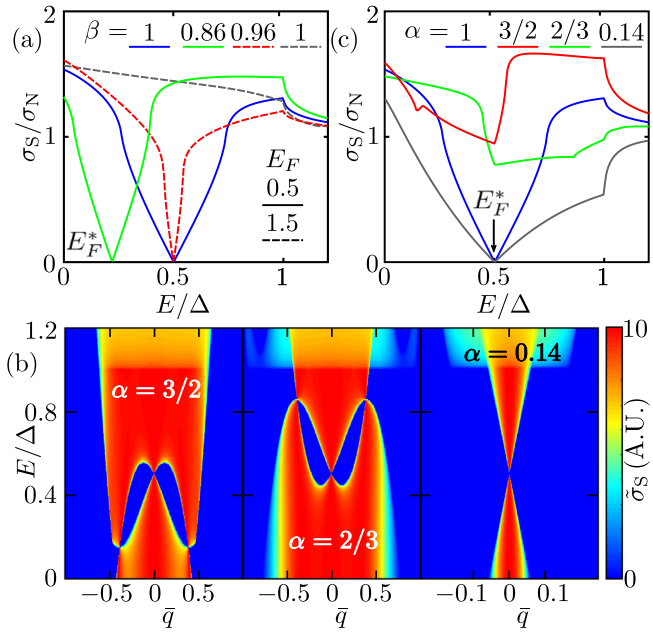

FIG. 4. Asymmetric superlattice potential characterized by parameters α and β as defined in the text. (a) Asymmetry in the height of the potential barriers and wells: for $\alpha = 1$ and $u/(2\pi) = 1.11$, differential conductance with different E_F^* and β. Dotted lines have $E_F = \Delta/2$, and solid lines have $E_F = 3\Delta/2$. (b), (c) Asymmetry in the width of the potential barriers and wells: (b) spectral differential conductance and (c) differential conductance for $\beta = 1$, $u/(2\pi) = 1.11$, and different values of α, adjusting E_F so that $E_F^* = \Delta/2$ in all cases. In all cases, $L = \xi_0/2$, and $\hbar v_F q_{\max} \simeq 15\Delta$ for the maps.

new DPs are created [see Fig. 4(a)]. For reference, we also plot in Fig. 4(a) a case with a symmetric SL potential taken from Fig. 3(b) (blue line). By changing the value of β, the conductance features a dip at different energies below the gap, as long as $E_F^* < \Delta$ (green line). If the asymmetry is such that $E_F^* > \Delta$, the conductance does not exhibit any dip and approaches the case of a heavily doped graphene layer, even if $E_F < \Delta$ (dashed gray line). The doping E_F of the graphene layer thus provides an experimentally controllable parameter that can rectify any asymmetry in the height of the barriers and wells of the SL potential.

B. Spatial asymmetry

When the asymmetry on the SL potential affects the widths of the barriers and wells ($\alpha \neq 1$), the impact on the conductance is more pronounced. In this situation, the position of the original DP is still given by E_F^*, but the new DPs appear at different energies. For example, the real doping E_F in the three panels in Fig. 4(b) has been adjusted so that all cases have $E_F^* = \Delta/2$. However, the barrier's width is bigger than the corresponding one for the wells in the left panel ($\alpha > 1$), while it is smaller in the other panels ($\alpha < 1$). As a result, the new DPs are created for energies below and above the effective Fermi energy E_F^*, respectively. In the right panel, the superlattice is so asymmetric that the new DPs merge back into the original Dirac cone, recovering the result for a heavily doped graphene layer.

The spatial asymmetry drastically changes the conductance, as we show in Fig. 4(c). As a reference, we show a symmetric result with finite doping $E_F = \Delta/2$ (blue line) and compare it to the asymmetric cases from Fig. 4(b), where the doping was adjusted so that $E_F^* = \Delta/2$. When $\alpha < 1$ (green line), the new DPs appear for energies bigger than the effective Fermi energy, and their impact on the conductance is diminished. On the other hand, if $\alpha > 1$ (red line), the new DPs appear for smaller energies and can be clearly seen as kinks in the conductance. The case with high asymmetry (gray line) approximates the conductance of a doped graphene layer with dominant intraband Andreev reflection [20].

Our results thus show the importance of a regularly spaced superlattice potential, while the asymmetry in the electrostatic barriers can be compensated by a uniform change in the doping level of the graphene layer.

C. Finite-length superlattice

The emergence of new Dirac points and their separation from the original cone in a semi-infinite SL potential can be discerned in the differential conductance by the parameter ε. We now analyze the impact of a finite-length SL potential on the previous results. A finite size in the vertical direction, parallel to the interfaces, would introduce additional structure due to the quantization of the parallel momentum. For simplicity, we consider only the infinite-width limit, where the vertical size is much larger than the horizontal length. The finite-length superlattice is then contacted on one side ($x = 0$) to a superconductor and on the other side ($x = -NL$) to a normal-state reservoir, which we model as a heavily doped graphene semi-infinite layer [35,36,46]. Here, L is the size of an n-p junction, and N is the total number of n-p junctions in the finite SL region. Nanoscale hybrid junctions where the reservoirs and the intermediate-scattering region are built from different materials present very different interface transmissions [50,51]. For simplicity, we consider here only transparent couplings between the finite SL and the normal and superconducting leads and a symmetric SL potential.

The finite length of the intermediate region results in the splitting of the continuous Dirac cone into energy bands [see Fig. 5(a)]. In the presence of a SL potential, the condition for the emergence of new DPs, $u = 2n\pi$, is roughly maintained even for a very small SL. A menorahlike pattern similar to that of Fig. 2(b) emerges for small lengths, although the resonances at the positions of the DPs are broadened and not so well defined. The broadening of the dispersion relation for subgap energies is shown in Fig. 5(a) for the undoped (left panel) and doped cases (right panel). The blurring of the DPs results in an increased probability of normal backscattering. We show the finite-length effect in the differential conductance in Figs. 5(b) and 5(c) for $E_F = 0$ and $\Delta/2$, respectively. For reference, the gray lines show the behavior of a semi-infinite superlattice potential with the same parameters. We confirm the robustness of the effect of the SL in the differential conductance for all energies different from E_F. At the charge neutrality point E_F, the semi-infinite case is qualitatively reproduced for superlattice lengths $N \gtrsim 50$, with $L = \xi_0/2$. However, to estimate the value of 2ε for a doped superlattice, only a few p-n junctions ($N \sim 20$) are needed.

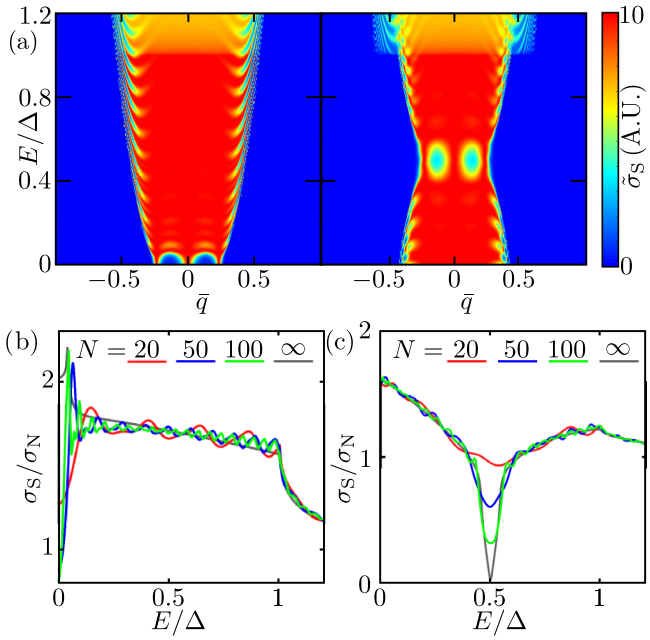

FIG. 5. Finite superlattice potential. (a) Spectral differential conductance for $N = 50$, with $E_F = 0$ (left) and $E_F = \Delta/2$ (right). In both cases $\hbar v_F q_{\max} \simeq 14\Delta$. Differential conductance for different numbers of n-p junctions N of the finite superlattice potential, with (b) $E_F = 0$ and (c) $E_F = \Delta/2$. The gray line recovers the semi-infinite superlattice potentials in Figs. 2 and 3. In all cases, $L = \xi_0/2$.

V. CONCLUSIONS

We have analyzed the transport properties of a graphene SL-S junction. We have demonstrated that the superlattice potential can create new DPs even in the presence of superconducting correlations. Moreover, the changes that the SL potential causes in graphene's spectrum are enhanced for subgap energies. Therefore, the emergence of new DPs can be monitored through the differential conductance of the junction. The normalized conductance features sharp changes for energy values equal to a parameter, ε, determined by the separation between newly created DPs and the original cone. Further, the superconducting conductance is always enhanced over the normal-state one for energies below but close to the gap Δ. These effects are robust in the presence of asymmetry in the superlattice potential and finite size, as long as the formation of new DPs is possible. Potential fluctuations due to charge inhomogeneity in graphene could be up to ∼5 meV [9]. We showed how changing the doping of the graphene layer by local gating could help correct the asymmetry in the superlattice potential induced by the charge inhomogeneity. Our results thus suggest that superconducting tunneling spectroscopy could be an interesting alternative to supercurrent measurements [52] to experimentally observe the modification of the band dispersion relation due to a superlattice potential on a graphene layer.

ACKNOWLEDGMENTS

We acknowledge funding from DIEB, Universidad Nacional de Colombia Project No. 34916, the Horizon 2020 research and innovation program under Marie Skłodowska-Curie Grant No. 743884, the Academy of Finland (Project No. 312299), and Spanish MINECO via Grants No. FIS2015-74472-JIN (AEI/FEDER/UE), No. FIS2014-55486P, and No. FIS2017-84860-R and through the "María de Maeztu" Program for Units of Excellence in R&D (Grant No. MDM-2014-0377).

APPENDIX A: SUPERLATTICE GREEN'S FUNCTION

To analyze the transport properties of the SL-S junction, we calculate the Green's function of the system. The building block for a semi-infinite graphene in the superlattice space is the Green's function of an isolated zigzag graphene layer finite in the x direction:

$$\hat{g}_0^{<(>)}(x,x') = \frac{-i}{2\hbar v_F\left(1 - r_L^B r_R^A\right)\cos\alpha} \times \left(e^{ik_x|x'-x|}\hat{f}_{\mp} + r_L^B r_R^A e^{-ik_x|x'-x|}\hat{f}_{\pm} + r_L^B e^{ik_x(x+x')}h_+ + r_R^A e^{-ik_x(x+x')}h_-\right), \quad \text{(A1)}$$

with

$$\hat{f}_{\pm} = \begin{pmatrix} 1 & \pm e^{\pm(-i\alpha)} \\ \pm e^{\pm i\alpha} & 1 \end{pmatrix}, \quad \hat{h}_{\pm} = \begin{pmatrix} e^{\pm(-i\alpha)} & \mp 1 \\ \pm 1 & -e^{\pm i\alpha} \end{pmatrix},$$

and

$$r_L^A = -e^{i\alpha}e^{-2ik_x x_L}, \quad r_R^A = -e^{-i\alpha}e^{2ik_x x_R},$$
$$r_L^B = e^{-i\alpha}e^{-2ik_x x_L}, \quad r_R^B = e^{i\alpha}e^{2ik_x x_R}.$$

Here, v_F is the Fermi velocity of the graphene sheet. The symbol $<(>)$ indicates $x < x'$ $(x > x')$. The explicit calculation of Eq. (A1) is given in Ref. [35].

One superlattice period (n-p junction) is composed of two finite graphene regions with different Fermi energies and widths $W_{p,n}$. The Green's function for each region is given by Eq. (A1), and they can be coupled using Dyson's equation to obtain the Green's function of the finite n-p junction. Assuming that the coupled region extends from $x_L = -L$ to $x_R = 0^-$, we obtain the Green's functions

$$\hat{g}_{np}^{>}(-L,-L) = \frac{-i}{\hbar v_F}\begin{pmatrix} -C_p & 0 \\ 1 & 0 \end{pmatrix}, \quad \text{(A2a)}$$

$$\hat{g}_{np}^{<}(-L,0^-) = \frac{-i}{\hbar v_F}\begin{pmatrix} 0 & -D_{pn} \\ 0 & 0 \end{pmatrix}, \quad \text{(A2b)}$$

$$\hat{g}_{np}^{<}(0^-,0^-) = \frac{-i}{\hbar v_F}\begin{pmatrix} 0 & -1 \\ 0 & -C_n \end{pmatrix}, \quad \text{(A2c)}$$

$$\hat{g}_{np}^{>}(0^-,-L) = \frac{-i}{\hbar v_F}\begin{pmatrix} 0 & 0 \\ -D_{pn} & 0 \end{pmatrix}. \quad \text{(A2d)}$$

The Green's function for a finite superlattice of length NL, with L being the period of an n-p junction, is obtained by coupling Eqs. (A2) to each other N times. The resulting Green's function reads

$$\tilde{g}_{fsl} = \frac{-i}{\hbar v_F}\begin{pmatrix} -C_n^N & 0 \\ 1 & 0 \end{pmatrix},$$
$$C_n^N = \frac{C_n^{N-1}t^2\left(C_p^{N-1} - D_{pn}^{N-1}\right) + C_p^{N-1}}{C_n^{N-1}C_p^{N-1}t^2 + 1}, \quad \text{(A3)}$$

where t describes the coupling between regions.

The Green's function of the semi-infinite superlattice is calculated using the self-similarity of a semi-infinite chain. Adding one block to a semi-infinite number of graphene *n-p* blocks results in the same semi-infinite chain. Therefore, it is possible to analytically calculate the Green's function for the complete superlattice evaluated at one edge $\hat{g}_{\rm SL}(0^-,0^-)$ by imposing that it is equal to the Green's function of the superlattice when a new block $\hat{g}_{np}$ has been added. Using Dyson's equation, we find

$$\hat{g}_{\rm SL}(0^-,0^-) = \hat{g}_{np}(0^-,0^-) - \hat{g}_{np}(0^-,-L)\hat{\Sigma}^\dagger \hat{M}^{-1}\hat{g}_{\rm SL}(-L,-L)\hat{\Sigma}\hat{g}_{np}(-L,0^-), \tag{A4}$$

with

$$\hat{M} = I - \hat{g}_{\rm SL}(-L,-L)\hat{\Sigma}\hat{g}_{np}(-L,-L)\hat{\Sigma}^\dagger,$$
$$\hat{\Sigma} = \tilde{t}\begin{pmatrix} 0 & 1 \\ 0 & 0 \end{pmatrix}.$$

Solving Eq. (A4), we obtain Eq. (4) of the main text.

APPENDIX B: DIFFERENTIAL CONDUCTANCE FOR THE SUPERLATTICE-SUPERCONDUCTOR JUNCTION

Once the Green's function for the coupled SL-S system is obtained, the electric current follows from the Keldysh formalism. Following the extension of the Hamiltonian approach described in Refs. [36,53], the zero-temperature differential conductance reads

$$\tilde{\sigma}_{\rm Q1} = t^2{\rm Tr}\left\{{\rm Re}\left[\left(\hat{I}+t\hat{G}^r_{t,ee}\sigma_1^T\right)\hat{\rho}_{sc,ee}\left(\hat{I}+t\sigma_1\hat{G}^{r*}_{t,ee}\right)\bar{\rho}_{sl,e}\right]\right\} + t^4{\rm Tr}\left[{\rm Re}\left(\hat{G}^{r*}_{t,eh}\bar{\rho}_{sl,e}\hat{G}^r_{t,eh}\sigma_1^T\hat{\rho}_{sc,hh}\sigma_1\right)\right], \tag{B1}$$

$$\tilde{\sigma}_{\rm Q2} = -t^3{\rm Tr}\left\{{\rm Re}\left[\left(\hat{I}+t\sigma_1\hat{G}^{r*}_{t,ee}\right)\bar{\rho}_{sl,e}\hat{G}^r_{t,eh}\sigma_1^T\hat{\rho}_{sc,he} + \left(\hat{I}+t\hat{G}^r_{t,ee}(E)\sigma_1^T\right)\hat{\rho}_{sc,eh}\sigma_1\hat{G}^{r*}_{t,eh}\bar{\rho}_{sl,e}\right]\right\}, \tag{B2}$$

$$\tilde{\sigma}_{\rm A} = t^4{\rm Tr}\left[{\rm Re}\left(\hat{G}^{r*}_{sc,eh}\bar{\rho}_{sl,e}\hat{G}^r_{sc,eh}\bar{\rho}_{sl,h} + \hat{G}^{r*}_{sc,he}\bar{\rho}_{sl,h}\hat{G}^r_{sc,he}\bar{\rho}_{sl,e}\right)\right], \tag{B3}$$

with $\bar{\rho}_{sl,e(h)} = \hat{\sigma}_1\hat{\rho}_{sl,ee(hh)}\hat{\sigma}_1^T$. The density of states ρ_{sl} and ρ_{sc} are related to the Green's functions of the decoupled system at equilibrium and are defined as $\rho(E) = \frac{i}{2\pi}(g-g^\dagger)$, where *sl* denotes the superlattice and *sc* is the superconductor at $x=0$.

The Green's functions of the coupled junction (SL-S), $\hat{G}^r_{sc,eh(he)}$ and $\hat{G}^r_{t,ee(eh)}$, are matrices in graphene sublattice space, representing elements in Nambu space. The coupling is realized via Dyson's equation as follows:

$$\tilde{G}^r_{sc} = \tilde{g}^r_{sc}(0^+,0^+) + \hat{G}^r_t\tilde{\Sigma}\tilde{g}^r_{sc}(0^+,0^+),$$
$$\tilde{G}^r_t = \tilde{g}^r_{sc}(0^+,0^+)\tilde{\Sigma}^\dagger\tilde{P}^{-1}\tilde{g}^r_{\rm SL}(0^-,0^-),$$
$$\tilde{P} = \hat{I} - \tilde{g}_{\rm SL}(0^-,0^-)\tilde{\Sigma}\tilde{g}_{sc}(0^+,0^+)\tilde{\Sigma}^\dagger,$$

where $\tilde{g}^r_{sc}(0^+,0^+)$ corresponds to the Green's function in equilibrium for the superconducting region and is given in Ref. [35].

In the case of a finite superlattice, the differential conductance is also given by Eq. (5), substituting the Green's function for the semi-infinite superlattice by a new function representing the coupling of a semi-infinite, heavily doped graphene contact, $\tilde{g}_{nc}$ (cf. Refs. [35,46]), with the finite superlattice $\tilde{g}_{fsl}$, Eq. (A3).

[1] S. Das Sarma, S. Adam, E. H. Hwang, and E. Rossi, Electronic transport in two-dimensional graphene, Rev. Mod. Phys. **83**, 407 (2011).

[2] A. V. Rozhkov, G. Giavaras, Y. P. Bliokh, V. Freilikher, and F. Nori, Electronic properties of mesoscopic graphene structures: Charge confinement and control of spin and charge transport, Phys. Rep. **503**, 77 (2011).

[3] T. O. Wehling, A. M. Black-Schaffer, and A. V. Balatsky, Dirac materials, Adv. Phys. **63**, 1 (2014).

[4] L. Brey and H. A. Fertig, Emerging Zero Modes for Graphene in a Periodic Potential, Phys. Rev. Lett. **103**, 046809 (2009).

[5] M. Barbier, P. Vasilopoulos, and F. M. Peeters, Extra Dirac points in the energy spectrum for superlattices on single-layer graphene, Phys. Rev. B **81**, 075438 (2010).

[6] P. Burset, A. Levy Yeyati, L. Brey, and H. A. Fertig, Transport in superlattices on single-layer graphene, Phys. Rev. B **83**, 195434 (2011).

[7] C.-H. Park, Y.-W. Son, L. Yang, M. L. Cohen, and S. G. Louie, Electron beam supercollimation in graphene superlattices, Nano Lett. **8**, 2920 (2008).

[8] R. Decker, Y. Wang, V. W. Brar, W. Regan, H.-Z. Tsai, Q. Wu, W. Gannett, A. Zettl, and M. F. Crommie, Local electronic properties of graphene on a BN substrate via scanning tunneling microscopy, Nano Lett. **11**, 2291 (2011).

[9] J. Xue, J. Sanchez-Yamagishi, D. Bulmash, P. Jacquod, A. Deshpande, K. Watanabe, T. Taniguchi, P. Jarillo-Herrero, and B. J. LeRoy, Scanning tunneling microscopy and spectroscopy of ultra-flat graphene on hexagonal boron nitride, Nat. Mater. **10**, 282 (2011).

[10] M. Yankowitz, J. Xue, D. Cormode, J. D. Sanchez-Yamagishi, K. Watanabe, T. Taniguchi, P. Jarillo-Herrero, P. Jacquod, and B. J. LeRoy, Emergence of superlattice Dirac points in graphene on hexagonal boron nitride, Nat. Phys. **8**, 382 (2012).

[11] L. A. Ponomarenko, R. V. Gorbachev, G. L. Yu, D. C. Elias, R. Jalil, A. A. Patel, A. Mishchenko, A. S. Mayorov, C. R. Woods, J. R. Wallbank, M. Mucha-Kruczynski, B. A. Piot, M. Potemski, I. V. Grigorieva, K. S. Novoselov, F. Guinea, V. I. Fal'ko, and A. K. Geim, Cloning of Dirac fermions in graphene superlattices, Nature (London) **497**, 594 (2013).

[12] M. Lee, J. R. Wallbank, P. Gallagher, K. Watanabe, T. Taniguchi, V. I. Fal'ko, and D. Goldhaber-Gordon, Ballistic miniband conduction in a graphene superlattice, Science **353**, 1526 (2016).

[13] Y. Cao, V. Fatemi, A. Demir, S. Fang, S. L. Tomarken, J. Y. Luo, J. D. Sanchez-Yamagishi, K. Watanabe, T. Taniguchi, E. Kaxiras, R. C. Ashoori, and P. Jarillo-Herrero, Correlated insulator behaviour at half-filling in magic-angle graphene superlattices, Nature (London) **556**, 80 (2018).

[14] Y. Cao, V. Fatemi, S. Fang, K. Watanabe, T. Taniguchi, E. Kaxiras, and P. Jarillo-Herrero, Unconventional superconductivity in magic-angle graphene superlattices, Nature (London) **556**, 43 (2018).

[15] P. Rickhaus, M. Weiss, L. Marot, and C. Schönenberger, Quantum Hall effect in graphene with superconducting electrodes, Nano Lett. **12**, 1942 (2012).

[16] V. E. Calado, S. Goswami, G. Nanda, M. Diez, A. R. Akhmerov, K. Watanabe, T. Taniguchi, T. M. Klapwijk, and L. M. K. Vandersypen, Ballistic Josephson junctions in edge-contacted graphene, Nat. Nanotechnol. **10**, 761 (2015).

[17] M. Ben Shalom, M. J. Zhu, V. I. Fal'ko, A. Mishchenko, A. V. Kretinin, K. S. Novoselov, C. R. Woods, K. Watanabe, T. Taniguchi, A. K. Geim, and J. R. Prance, Quantum oscillations of the critical current and high-field superconducting proximity in ballistic graphene, Nat. Phys. **12**, 318 (2016).

[18] G.-H. Lee and H.-J. Lee, Proximity coupling in superconductor-graphene heterostructures, Rep. Prog. Phys. **81**, 056502 (2018).

[19] C. W. J. Beenakker, Colloquium: Andreev reflection and Klein tunneling in graphene, Rev. Mod. Phys. **80**, 1337 (2008).

[20] C. W. J. Beenakker, Specular Andreev Reflection in Graphene, Phys. Rev. Lett. **97**, 067007 (2006).

[21] D. K. Efetov, L. Wang, C. Handschin, K. B. Efetov, J. Shuang, R. Cava, T. Taniguchi, K. Watanabe, J. Hone, C. R. Dean, and P. Kim, Specular interband Andreev reflections at van der Waals interfaces between graphene and $NbSe_2$, Nat. Phys. **12**, 328 (2016).

[22] T. Dirks, T. L. Hughes, S. Lal, B. Uchoa, Y.-F. Chen, C. Chialvo, P. M. Goldbart, and N. Mason, Transport through Andreev bound states in a graphene quantum dot, Nat. Phys. **7**, 386 (2011).

[23] Z. B. Tan, D. Cox, T. Nieminen, P. Lähteenmäki, D. Golubev, G. B. Lesovik, and P. J. Hakonen, Cooper Pair Splitting by Means of Graphene Quantum Dots, Phys. Rev. Lett. **114**, 096602 (2015).

[24] C. Tonnoir, A. Kimouche, J. Coraux, L. Magaud, B. Delsol, B. Gilles, and C. Chapelier, Induced Superconductivity in Graphene Grown on Rhenium, Phys. Rev. Lett. **111**, 246805 (2013).

[25] B. M. Ludbrook, G. Levy, P. Nigge, M. Zonno, M. Schneider, D. J. Dvorak, C. N. Veenstra, S. Zhdanovich, D. Wong, P. Dosanjh, C. Straßer, A. Stöhr, S. Forti, C. R. Ast, U. Starke, and A. Damascelli, Evidence for superconductivity in Li-decorated monolayer graphene, Proc. Natl. Acad. Sci. USA **112**, 11795 (2015).

[26] J. Chapman, Y. Su, C. A. Howard, D. Kundys, A. N. Grigorenko, F. Guinea, A. K. Geim, I. V. Grigorieva, and R. R. Nair, Superconductivity in Ca-doped graphene laminates, Sci. Rep. **6**, 23254 (2016).

[27] A. P. Tiwari, S. Shin, E. Hwang, S.-G. Jung, T. Park, and H. Lee, Superconductivity at 7.4 K in few layer graphene by Li-intercalation, J. Phys.: Condens. Matter **29**, 445701 (2017).

[28] A. Di Bernardo, O. Millo, M. Barbone, H. Alpern, Y. Kalcheim, U. Sassi, A. K. Ott, D. De Fazio, D. Yoon, M. Amado, A. C. Ferrari, J. Linder, and J. W. A. Robinson, p-wave triggered superconductivity in single-layer graphene on an electron-doped oxide superconductor, Nat. Commun. **8**, 14024 (2017).

[29] G.-H. Lee, G.-H. Park, and H.-J. Lee, Observation of negative refraction of Dirac fermions in graphene, Nat. Phys. **11**, 925 (2015).

[30] V. V. Cheianov, V. Fal'ko, and B. L. Altshuler, The focusing of electron flow and a Veselago lens in graphene p-n junctions, Science **315**, 1252 (2007).

[31] J. Cserti, A. Pályi, and C. Péterfalvi, Caustics Due to a Negative Refractive Index in Circular Graphene *p-n* Junctions, Phys. Rev. Lett. **99**, 246801 (2007).

[32] Y. Xing, J. Wang, and Q.-F. Sun, Focusing of electron flow in a bipolar graphene ribbon with different chiralities, Phys. Rev. B **81**, 165425 (2010).

[33] A. G. Moghaddam and M. Zareyan, Graphene-Based Electronic Spin Lenses, Phys. Rev. Lett. **105**, 146803 (2010).

[34] S. Gómez, P. Burset, W. J. Herrera, and A. Levy Yeyati, Selective focusing of electrons and holes in a graphene-based superconducting lens, Phys. Rev. B **85**, 115411 (2012).

[35] W. J. Herrera, P. Burset, and A. Levy Yeyati, A Green function approach to graphene-superconductor junctions with well-defined edges, J. Phys.: Condens. Matter **22**, 275304 (2010).

[36] O. E. Casas, S. Gómez Páez, A. Levy Yeyati, P. Burset, and W. J. Herrera, Subgap states in two-dimensional spectroscopy of graphene-based superconducting hybrid junctions, Phys. Rev. B **99**, 144502 (2019).

[37] W. L. McMillan, Theory of superconductor-normal metal interfaces, Phys. Rev. **175**, 559 (1968).

[38] A. Furusaki and M. Tsukada, Dc Josephson effect and Andreev reflection, Solid State Commun. **78**, 299 (1991).

[39] S. Kashiwaya and Y. Tanaka, Tunnelling effects on surface bound states in unconventional superconductors, Rep. Prog. Phys. **63**, 1641 (2000).

[40] B. Lu, P. Burset, K. Yada, and Y. Tanaka, Tunneling spectroscopy and Josephson current of superconductor-ferromagnet hybrids on the surface of a 3d TI, Supercond. Sci. Technol. **28**, 105001 (2015).

[41] F. Crépin, P. Burset, and B. Trauzettel, Odd-frequency triplet superconductivity at the helical edge of a topological insulator, Phys. Rev. B **92**, 100507(R) (2015).

[42] P. Burset, B. Lu, G. Tkachov, Y. Tanaka, E. M. Hankiewicz, and B. Trauzettel, Superconducting proximity effect in three-dimensional topological insulators in the presence of a magnetic field, Phys. Rev. B **92**, 205424 (2015).

[43] F. Keidel, P. Burset, and B. Trauzettel, Tunable hybridization of Majorana bound states at the quantum spin Hall edge, Phys. Rev. B **97**, 075408 (2018).

[44] B. Lu and Y. Tanaka, Study on Green's function on topological insulator surface, Philos. Trans. R. Soc. A **376**, 20150246 (2018).

[45] D. Breunig, P. Burset, and B. Trauzettel, Creation of Spin-Triplet Cooper Pairs in the Absence of Magnetic Ordering, Phys. Rev. Lett. **120**, 037701 (2018).

[46] P. Burset, A. L. Yeyati, and A. Martín-Rodero, Microscopic theory of the proximity effect in superconductor-graphene nanostructures, Phys. Rev. B **77**, 205425 (2008).

[47] P. Burset, W. Herrera, and A. Levy Yeyati, Proximity-induced interface bound states in superconductor-graphene junctions, Phys. Rev. B **80**, 041402(R) (2009).

[48] P. Burset, W. J. Herrera, and A. Levy Yeyati, Formation of interface bound states on a graphene-superconductor junction

in the presence of charge inhomogeneities, Graphene **02**, 35 (2013).

[49] D. P. Arovas, L. Brey, H. A. Fertig, E.-A. Kim, and K. Ziegler, Dirac spectrum in piecewise constant one-dimensional (1d) potentials, New J. Phys. **12**, 123020 (2010).

[50] T. Klapwijk and S. Ryabchun, Direct observation of ballistic Andreev reflection, J. Exp. Theor. Phys. **119**, 997 (2014).

[51] J. Wiedenmann, E. Liebhaber, J. Kübert, E. Bocquillon, P. Burset, C. Ames, H. Buhmann, T. M. Klapwijk, and L. W. Molenkamp, Transport spectroscopy of induced superconductivity in the three-dimensional topological insulator HgTe, Phys. Rev. B **96**, 165302 (2017).

[52] D. I. Indolese, R. Delagrange, P. Makk, J. R. Wallbank, K. Wanatabe, T. Taniguchi, and C. Schönenberger, Signatures of Van Hove Singularities Probed by the Supercurrent in a Graphene-Hbn Superlattice, Phys. Rev. Lett. **121**, 137701 (2018).

[53] J. C. Cuevas, A. Martín-Rodero, and A. L. Yeyati, Hamiltonian approach to the transport properties of superconducting quantum point contacts, Phys. Rev. B **54**, 7366 (1996).